https://doi.org/10.5194/tc-2021-348
Preprint. Discussion started: 24 November 2021

The Cryosphere Discussions

Calibration of basal melt on past ice discharge lowers projections of Antarctica's sea level contribution

Eveline C. van der Linden[1], Dewi Le Bars[1], Erwin Lambert[1], and Sybren Drijfhout[1,2]

[1]Royal Netherlands Meteorological Institute, Utrechtseweg 297, 3731 GA, De Bilt, The Netherlands
[2]Institute for Marine and Atmospheric Research Utrecht, Department of Physics, Utrecht University, Princetonplein 5, 3584 CC, Utrecht, The Netherlands

Correspondence: Eveline C. van der Linden (linden@knmi.nl)

Abstract. Antarctic mass loss is the largest contributor to uncertainties in sea level projections on centennial timescales. In this study the contribution of Antarctica's ice discharge to future sea level changes is computed with ocean thermal forcing from 14 earth system models and linear response functions from 16 ice sheet models for three greenhouse gas emission scenarios. Different than in previous studies, basal melt was calibrated on observed Antarctic ice discharge rather than on basal melt itself with an iterative approach. For each model combination, a linear and quadratic melt dependency were calibrated both regionally (in five Antarctic sectors) and at the continental scale. Projections using all model combinations show that the variation in basal melt computation methods affect the projected sea level more than the scenario variations (SSP1-2.6 to SSP5-8.5). After calibration, a high number of model pairs still underestimated ice discharge in hindcasts over 1979-2017. Therefore top 10% best-performing model combinations were selected for each method. A comparison between these model selections shows that the quadratic melt parameterisation with Antarctic-wide calibration performs best in reproducing past ice discharge. We conclude that calibration of basal melt on past ice discharge combined with model selection makes projections of Antarctic ice discharge (more) consistent with observations over the past four decades. Moreover, calibration of basal melt on past ice discharge results in lower basal melt sensitivities and thus lower projections of Antarctica's sea level contribution than estimates of previous multi-model studies.

1 Introduction

Sea level rise poses an increasing threat to densely populated coasts and deltas worldwide (Hinkel et al., 2014). Even if the 1.5 degree target of the Paris Agreement is met, global mean sea level will rise several meters in the longer term (Clark et al., 2016; Fox-Kemper et al., 2021). At present, a global acceleration of sea level rise is visible in satellite measurements and the sea level is already rising more than twice as fast as the average rate over the twentieth century (Nerem et al., 2018; Dangendorf et al., 2019).

Mass loss from land ice is currently accelerating and is now (over the period 2006–2018) the largest contributor to the global mean sea level rise (Fox-Kemper et al., 2021). Antarctic ice sheet mass loss has tripled over the last decade (Shepherd et al., 2018), which can be mainly attributed to increased ice discharge in the Amundsen Sea (Rignot et al., 2019). Models and geological data indicate that the Antarctic ice sheet will cause most of the sea level rise in the long term (Bamber et al.,

https://doi.org/10.5194/tc-2021-348
Preprint. Discussion started: 24 November 2021

2019). Moreover, melt of land ice is the largest contributor to uncertainties on centennial timescales (Palmer et al., 2020; van de Wal et al., 2019). The degree of acceleration of future sea level changes is mainly determined by dynamic processes on the Antarctic ice sheet. The underlying processes are 1) increased melt from below by warmer ocean water (basal melt) and 2) increased calving (iceberg formation) triggered by basal melt and/or surface melt (Rignot and Jacobs, 2002; Pritchard et al., 2012; Liu et al., 2015; van den Broeke, 2005). It is important to gain a better understanding of the many uncertainties about the Antarctic contribution to sea level rise that exist and to reduce these uncertainties when possible to support adaptation planning (Haasnoot et al., 2020). Uncertainties associated with the Antarctic contribution to sea level rise even appear to be increasing. Using similar methodologies, the estimated Antarctic contribution in Levermann et al. (2020) shows increased uncertainty compared to its previous study (Levermann et al., 2014) and expert judgment assessments of Bamber et al. (2019) give higher uncertainties than before (Bamber and Aspinall, 2013). To address this issue our study aims to gain more insight in the Antarctic contribution to and uncertainties in future sea level changes and provides directions for reducing these uncertainties.

Future projections of Antarctic mass loss are often based on modelling studies. Most earth system models (ESMs) do not have interactive ice sheet modules, because ice sheet models are particularly sensitive to small changes in the climate and often assume unrealistic geometries if they have to be balanced with the data from ESMs. This means that changes in the mass loss of an ice sheet are not (properly) predicted by ESMs and that ice sheets in coupled ice sheet-ESMs show undesirable and unrealistic trends. The proper functioning of ice sheet models in an earth system model is a worldwide effort for which no effective solution can be expected in the short term. Therefore, ice sheet models are often used as a standalone unit and balanced with observations. In this setup the forcing of ice sheet models is provided by ESMs.

Over the last decade, ice sheet modelling has advanced from single model studies to model intercomparison projects (MIPs). In these projects, earth system modelling and ice sheet modelling are combined to make projections of land ice. The Ice Sheet MIP (ISMIP) (Nowicki et al., 2016) and Linear Antarctic Response MIP (LARMIP) (Levermann et al., 2020) are currently used as a basis for projections of the Antarctic land ice evolution (Fox-Kemper et al., 2021). ISMIP6 (Seroussi et al., 2020) provides process-based projections of the sea level contribution of the Antarctic ice sheet based on a variety of ice sheet models that are forced by atmosphere and ocean output from CMIP5 ESMs. ISMIP6 made a selection of six ESMs based on two main criteria. The first criterion is based on their performance in reproducing current climate (atmosphere and ocean) near Antarctica. The second criterion ensures that the ESM selection includes a diversity of warming rates over the 21st century so that the uncertainty-range in projections is captured (Barthel et al., 2020; Nowicki et al., 2020). One risk of the second criterion is that models with a relatively bad performance over the historical period in terms of trends could have been chosen. Bias metrics for the selection included criteria on the mean state of the ocean and atmosphere, but did not include trends. In ISMIP6 basal melt was chosen to depend quadratically on thermal forcing (Favier et al., 2019) and is calibrated on basal melt observations in two regions (mean Antarctic ice sheet and the Pine Island Glacier grounding line) (Jourdain et al., 2020). LARMIP-2 focuses on ice sheet mass loss due to ice shelf basal melt (Levermann et al., 2014, 2020). In that study the temperature melt-relation is parameterised with a linear dependency on thermal forcing. ISMIP6 and LARMIP-2 have thirteen ice sheet models in common and are primarily based on the CMIP5 models and scenarios (RCPs) as forcing. Edwards et al. (2021) estimated probability

https://doi.org/10.5194/tc-2021-348
Preprint. Discussion started: 24 November 2021

distributions for projections under the new SSP scenarios based on CMIP6 ESMs, by using statistical emulation of the ISMIP6 ice sheet models.

Our study follows LARMIP-2 to account for the sensitivity of ice sheet models to climate change by using linear response functions (RF) of ice sheet models. The LARMIP-2 RFs were obtained by prescribing for five regions an immediate change in basal melt of the ice sheet and simulating the resulting increase in ice sheet discharge with the ice sheet model. In this way a relationship between basal melt and mass loss is obtained for each region. Another relationship between thermal forcing and basal melt is used to compute basal melt from ocean temperatures. These relationships, together with a time-dependent warming, then lead to a time-dependent mass loss of the ice sheet. This method was applied by Levermann et al. (2014, 2020) to a number of ice sheet models. In those studies, CMIP5 models were used to diagnose the relationship between global surface air temperature (GSAT) and ocean temperature changes around Antarctica, and GSAT was used as a driver of the method. The current study improves this step by using subsurface ocean temperature as driver (Lambert et al., 2021). In addition to the linear melt dependency as in the Levermann et al. (2020) study, a more advanced quadratic basal melt parameterisation is applied since observation-based evidence suggests a nonlinear relationship between melting and ocean temperature (Jenkins et al., 2018). The basal melt parameterisations are calibrated on observation-based estimates of ice discharge (Rignot et al., 2019), rather than on basal melt as is done in ISMIP6. As calibration target the mass loss estimates of Rignot et al. (2019) were chosen over Shepherd et al. (2018) for two reasons. The first reason is that Rignot et al. does not include surface mass balance processes which makes the data directly comparable with our results. The second reason is that the Rignot et al. record starts earlier which allows us to look into mass loss acceleration during a longer period. Two different calibrations are applied: at the regional and continental scale. Using different warming scenarios and RFs for a variety of models, we arrive at an estimate of the future mass loss of Antarctica that is consistent with observed mass loss over the past four decades.

2 Methodology

In this study the contribution of Antarctica's ice discharge to sea level changes is computed with state-of-the-art ESMs from Coupled Model Intercomparison Project Phase 6 (CMIP6; Eyring et al. 2016) and linear response functions from the Linear Antarctic Response MIP (LARMIP-2; Levermann et al. 2020) ice sheet models.

The basic procedure of this study follows that of Levermann et al. (2020) with a number of modifications as explained below and illustrated in Fig. 1. Earth system models from CMIP6 are used as a basis for the computations, guaranteeing implementation of state-of-the-art models in the analysis and projections. Ocean temperatures are directly taken from the CMIP6 models, instead of estimating them from scaling coefficients and global mean air temperature. For the representation of basal melt our method employs a linear as well as a quadratic melt relation with thermal forcing (TF), i.e. the difference between the in situ temperature of sea water (T_o) and the in situ freezing-melting point temperature (T_f):

$$TF = T_o - T_f. \tag{1}$$

Finally, the parameterisations are calibrated on regional or Antarctic-wide observed ice discharge from Rignot et al. (2019). This calibration step is a key difference with the Levermann et al. studies.

https://doi.org/10.5194/tc-2021-348
Preprint. Discussion started: 24 November 2021

The Cryosphere Discussions
Open Access
EGU

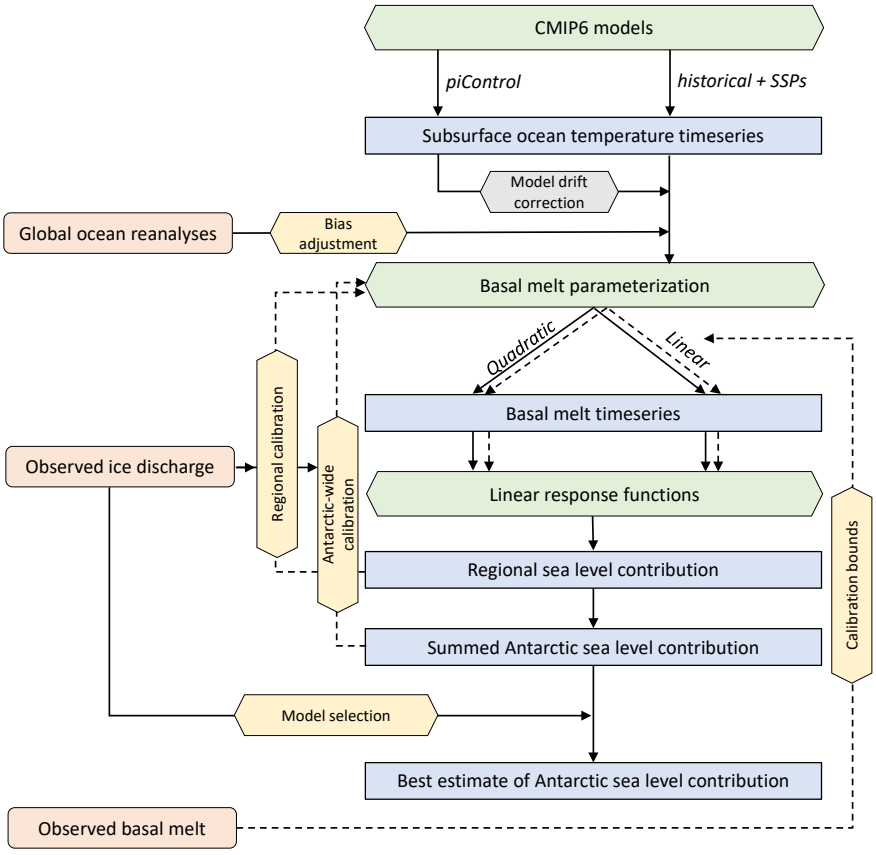

Figure 1. Flow diagram of procedure. Observational constraints are indicated in orange, main computations of the Levermann et al. method in green (including model experiments by the modelling groups), calibration methods in yellow, bias-adjustment in grey and (intermediate) output data in blue. The continuous lines represent direct pathways while the dashed lines refer to iterative processes or optional choices during calibration.

2.1 Ocean forcing

The ocean forcing consists of annual mean simulated subsurface ocean temperatures by CMIP6 ESMs. The ocean temperatures are taken from the historical experiment (1850-2014) and the Shared Socioeconomic Pathways (SSP) SSP1-2.6, SSP2-4.5 and SSP5-8.5 (2015-2100). Only models that have data available at the Earth System Grid Federation (ESGF) data server for the historical experiment and all three SSP scenarios (at the time of study) are considered. In addition, models should provide data for the full period (1850-2100) without any data gaps since the computation of the delayed ice sheet response requires a continuous time series. Table 1 summarises which models have been taken into account.

https://doi.org/10.5194/tc-2021-348
Preprint. Discussion started: 24 November 2021


The Cryosphere Discussions

Table 1. CMIP6 models that have been evaluated. For each region the subsurface ocean temperature bias (in K) compared to the GREP reanalysis is indicated over the period 1993-2018, including years 2015-2018 for the SSP2-4.5 scenario. The 'drift correction' column indicates whether the piControl experiment was used for model drift correction or the historical experiment.

CMIP6 model	EAIS	Weddell	Amundsen	Ross	Peninsula	Drift correction
ACCESS-CM2	-0.33	-0.11	-1.05	-1.26	0.09	historical
CAMS-CSM1-0	0.24	-0.05	0.22	-0.94	0.39	piControl
CAS-ESM2-0	1.43	0.79	0.20	-0.18	2.18	historical
CMCC-ESM2	0.31	-0.23	0.51	-0.10	0.58	piControl
CanESM5	-0.55	-0.43	-0.07	-0.80	-0.21	piControl
EC-Earth3	0.06	-0.57	1.17	0.71	-0.33	historical
EC-Earth3-Veg	-0.10	-0.58	0.84	0.44	-0.34	piControl
GFDL-ESM4	0.05	-0.38	0.45	-1.00	0.20	piControl
INM-CM4-8	-0.37	0.32	-0.66	-0.17	0.19	piControl
INM-CM5-0	-0.74	-0.24	-1.16	-1.11	-0.16	piControl
MIROC6	0.81	0.55	1.58	1.40	0.29	historical
MPI-ESM1-2-LR	-0.31	0.03	0.08	-0.59	-0.41	piControl
MRI-ESM2-0	-0.12	-0.10	-0.12	-0.31	0.32	historical
NorESM2-MM	-0.92	-0.45	-0.71	-0.84	-0.74	piControl
Mean	-0.04	-0.10	0.09	-0.34	0.15	-
Std	0.59	0.40	0.78	0.74	0.67	-

Table 2. Mean ice shelf depth (in m) for the five sectors in Fig. 2.

Sector	Depth (m)
EAIS	369
Weddell	420
Amundsen	305
Ross	312
Peninsula	420

Ocean temperatures are averaged over five oceanic sectors: the East Antarctic Ice Sheet (EAIS), Ross, Amundsen, Weddell and Peninsula sector (Fig. 2), and averaged vertically over a range of 100 m, centered around the depth of the ice shelf base (Table 2). Different from Levermann et al. (2020), the Peninsula sector is defined as a separate ocean sector rather than using the same ocean sector coordinates as the Amundsen sector.

https://doi.org/10.5194/tc-2021-348
Preprint. Discussion started: 24 November 2021

The Cryosphere Discussions
Open Access
EGU

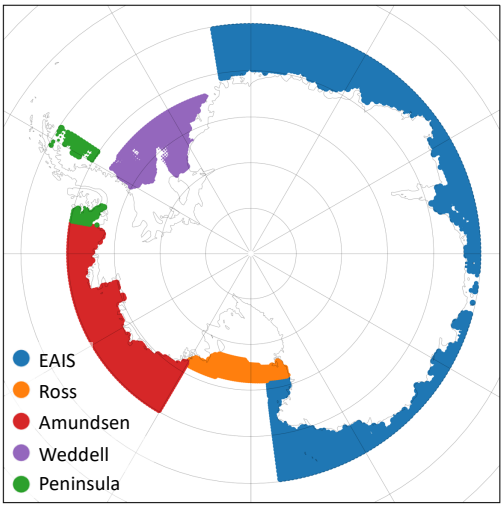

Figure 2. Ocean sector definition.

The time series are corrected for model drift by removing the long term trend diagnosed by the linear trend in the pre-industral control (piControl) experiment (Fig. 3). For models that did not provide suitable data for the piControl experiment, the model drift is estimated from the historical experiment with a variable detrending period starting in 1850 and ending between 1900 and 1950. The smallest absolute trend within this period is considered model drift and removed from the time series. In this way we assure that (multi-)decadal variability has minimal influence on the trend magnitude. For the quadratic melt parameterisaton, the resulting temperatures are bias-adjusted with global ocean reanalyses called the Global Reanalysis Ensemble Product (GREP). GREP can be obtained from the Copernicus Marine Server at 1 degree horizontal resolution over the period during which altimetry data observations are available (1993-2018). It is constructed by postprocessing of four reanalyses: GLORYS2V4 from Mercator Ocean (France), ORAS5 from ECMWF, FOAM/GloSea5 from Met Office (UK), and C-GLORS05 from CMCC (Italy). Although the ocean temperature bias has no clear relation with projected temperature trends in ESMs (Little and Urban, 2016), it affects the magnitude of basal melt in the quadratic parameterisation. Therefore, before computing the basal melt the ocean temperatures are bias-corrected. It should be noted, however, that the reanalysis data may also be biased due to a paucity of assimilated data and the absence of ice shelves in the physical ocean models. Averaged over all CMIP6 models the subsurface temperature of the CMIP6 multi-model mean is cold-biased for the EAIS, Weddell and Ross sectors over the 1993-2018 period. For the Amundsen and Peninsula sectors the mean simulated temperature is warm-biased (Table 1). For all regions, the sign of the bias differs between individual models. The ensemble mean bias over the 1993-2018 time period is removed from the modelled ocean temperatures over the entire historical and future period to obtain the bias-adjusted ocean temperatures (Fig. 3).

https://doi.org/10.5194/tc-2021-348
Preprint. Discussion started: 24 November 2021

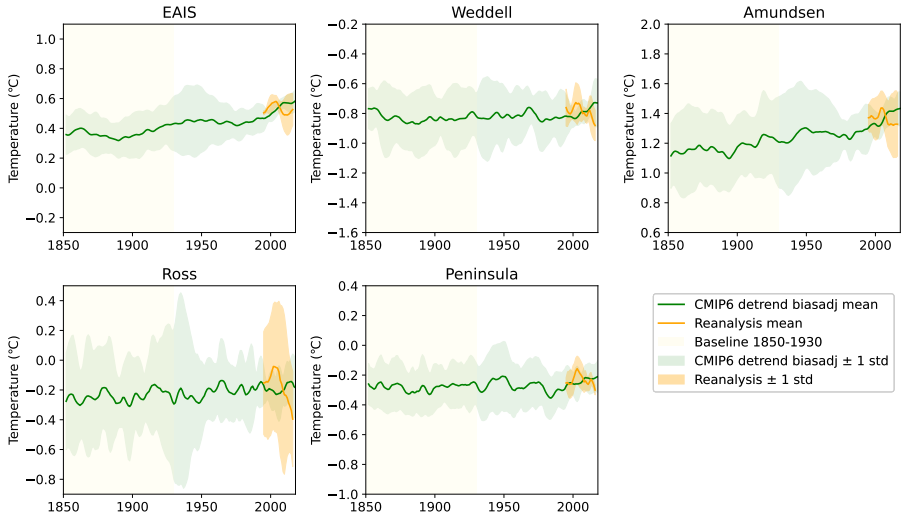

Figure 3. Annual mean subsurface ocean temperature time series smoothed by a five-year running average filter for the model drift- and bias-adjusted (green) CMIP6 multi-model mean and the GREP ensemble mean (orange). For CMIP6 models, the historical experiment (1850-2014) is combined with SSP2-4.5 (2015-2018) for this visualisation. Note that the tick distances of the vertical axis are the same for all regions, but the ranges are different.

2.2 Basal melt parameterisation

Warming of ocean water above the freezing point temperature in ice shelf cavities induces basal melt of the corresponding ice shelves. CMIP6 models, however, typically do not represent ice shelf cavities and the related thermal and dynamical properties. Coastal ocean temperatures should therefore be translated into these cavities. This can be done by using a parameterisation that relates the far-field (coastal) ocean temperature to basal melt. Most of the simple basal melt parameterisations assume a relation with thermal forcing. Our method employs a linear and quadratic melt relation with thermal forcing (Table 3). The quadratic relation was suggested to outperform a linear relation (Favier et al., 2019), but we will apply both so that we can compare our results with the linear relation used in Levermann et al. (2020). The linear relation is defined as:

$$m = \gamma \left(\frac{\rho_{sw} c_{po}}{\rho_i L_i} \right) TF, \tag{2}$$

It assumes a constant heat exchange, independent on the local stratification and circulation. The quadratic relation is defined as:

$$m = \gamma \left(\frac{\rho_{sw} c_{po}}{\rho_i L_i} \right)^2 TF|TF|. \tag{3}$$

where m is the basal melt and γ is the calibration parameter. The quadratic relation assumes that the heat exchange scales with the buoyancy-driven cavity circulation and that this scales linearly with the large-scale temperature gradient. The values of the physical constants ρ_{sw}, c_{po}, ρ_i and L_i are given in Table 4. The freezing-melting point temperature T_f underneath ice shelves

https://doi.org/10.5194/tc-2021-348
Preprint. Discussion started: 24 November 2021


The Cryosphere Discussions

Table 3. Abbreviations for basal melt parameterisation and calibration methods. Two different basal melt parameterisation methods were employed: linear and quadratic. Each parameterisation has been calibrated Antarctic wide and regionally. Unbounded means that γ has zero as lower limit and no upper limit for at least 95% of the ESM-RF combinations. Bounded means that the Levermann et al. (2020) bounds are applied on the linear parameterisation (both upper and lower bounds).

Abbreviation	Parameterisation	Calibration bounds	Calibration region
QUR	Quadratic	Unbounded	Regional
QUA	Quadratic	Unbounded	Antarctic
LUR	Linear	Unbounded	Regional
LUA	Linear	Unbounded	Antarctic
LBR	Linear	Bounded	Regional
LBA	Linear	Bounded	Antarctic

is computed from the ocean salinity S_o and the depth of the ice shelf base z_b:

$$T_f = \lambda_1 S_o + \lambda_2 + \lambda_3 z_b. \tag{4}$$

See Table 4 for the values of the physical constants. Favier et al. take T_o and T_f either as local or nonlocal values, where nonlocal is the product of local and nonlocal (averaged over the entire ice draft of a given sector) thermal forcing. In the current study, a purely nonlocal forcing is applied, similar to DeConto and Pollard (2016) and Levermann et al. (2020). The values of T_o are computed as averages over the five (far-field) oceanic sectors, around the depth of the ice shelf base (see Table 2). Since most CMIP6 models do not resolve cavities, the far-field ocean temperature is taken. The underlying assumption is that the ocean temperature remains constant while it is advected into the cavity. Also note that the ocean sectors are somewhat wider than the continental shelf, consistent with Levermann et al. (2020). The advantage of a wider region is that it allows for more assimilated observations in the reanalysis product that is used for the bias adjustment of ocean temperature (the continental shelf region is only sparsely sampled). Furthermore, the resolution of most CMIP6 models is not high enough to resolve the ocean circulation on the continental shelf, including the Antarctic Slope Current (Thompson et al., 2018). The computation of T_f is based on a constant salinity value for each oceanic sector, which is computed from the far-field salinity climatology of the reanalysis data. The resulting values of T_f are approximately -1.6 °C in each sector.

Note that the melt is positive if the ocean temperature exceeds the freezing-melting point temperature and negative (i.e. water is refreezing) otherwise. The change in basal melt anomaly is defined as the difference in basal melt between time t and the baseline time period, 1850-1930. This period was chosen since it is long enough to reduce the impact of natural variability on the baseline but short enough so that it doesn't include the trends due to anthropogenic forcing.

Basal melt anomalies in linear parameterisations do not depend on the mean temperature, only on the anomaly. In contrast, basal melt computed from the quadratic parameterisation depend on the mean temperature as well. As a consequence, biases in ocean temperature will influence the estimated magnitude of basal melt changes. Ocean temperatures were therefore bias-

https://doi.org/10.5194/tc-2021-348
Preprint. Discussion started: 24 November 2021


The Cryosphere Discussions
Open Access
EGU

Table 4. Physical constants.

parameter	symbol	value	unit
ice density	ρ_i	917	kg m^{-3}
sea water density	ρ_{sw}	1028	kg m^{-3}
specific heat capacity of ocean mixed layer	c_{po}	3947	J kg^{-1} K^{-1}
latent heat of fusion of ice	L_i	3.34×10^5	J kg^{-1}
heat exchange velocity	γ	calibrated	m s^{-1}
liquidus slope	λ_1	-0.0575	°C PSU^{-1}
liquidus intercept	λ_2	0.0832	°C
liquidus pressure coefficient	λ_3	7.59×10^{-4}	°C m^{-1}

adjusted with the ocean reanalysis data. The basal melt parameterisation can be calibrated with the heat exchange velocity γ. It should be noted that γ has a different order of magnitude in the linear and quadratic parameterisation and is not directly comparable.

2.3 Sea level contribution and calibration

Linear response functions (RFs) from LARMIP-2 will be used to compute the cumulative sea level contribution ΔS (in meters) due to a change in basal melt for each of the five sectors:

$$\Delta S(t) = \int_0^t d\tau \; \Delta m(\tau) \cdot RF(t-\tau). \tag{5}$$

LARMIP-2 provides RFs of 16 ice sheet models. Combined with the 14 ESMs (Table 1), this results in 224 ESM-RF combinations for the projections. The resulting sea level contributions are calibrated on observation-based ice discharge. For each individual sector and the total Antarctic, we have derived the observed ice discharge from Rignot et al. (2019) data. Then the root-mean-square error (RMSE) between the observed and modelled cumulative ice discharge for each ESM-RF combination is determined over a wide range of γ values. The RMSE is computed over the full time series to constrain models on the cumulative sea level change as well as the acceleration. For all calibrations, γ should be equal or greater than zero, since negative values would imply that temperatures above the melting point lead to ice growth, which is deemed not physically possible. The γ value giving the lowest RMSE for each ESM-RF pair provides the calibrated γ (Fig. 5).

The linear basal melt parameterisation has been calibrated in two ways: with bounded and unbounded γ values (Table 3). For the 'unbounded' calibrations, the upper bound of the γ range is determined by the requirement that at least 95% of all ESM-RF combinations should have the best fit within the γ range; they have no upper bound. This means that for at most 5% of the ESM-RF pairs there is an upper bound. This resulted in a γ range of 0.0-6.0 m yr^{-1} for the quadratic parameterisation and 0.0-0.1 m yr^{-1} for the linear parameterisation. In order to compare our results to Levermann et al. (2020), we also applied

https://doi.org/10.5194/tc-2021-348
Preprint. Discussion started: 24 November 2021

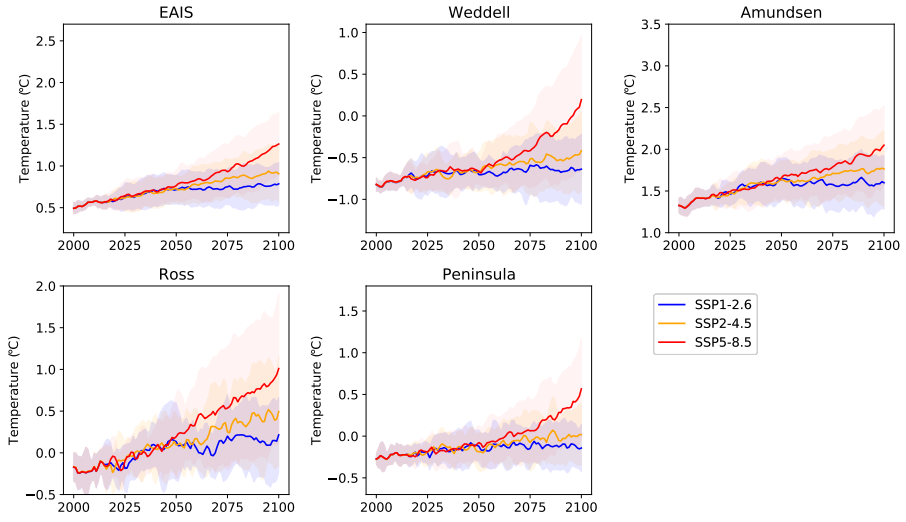

Figure 4. Projections of annual mean subsurface ocean temperature for SSP1-2.6, SSP2-4.5 and SSP5-8.5 including all evaluated CMIP6 models (Table 1). The shaded regions indicate one associated intermodel standard deviation. Note that the tick distances of the vertical axis are the same for all regions, but the ranges are different.

a bounded calibration. For the bounded calibration, the basal melt sensitivity (i.e. $\gamma\left(\frac{\rho_{sw}c_{po}}{\rho_i L_f}\right)$) should be in the empirically based range determined by Levermann et al. (2020): 7-16 m yr^{-1} K^{-1}. The bounded calibration is only applied to the linear parameterisation.

The calibration is applied regionally and Antarctic-wide (Table 3). For each ESM-RF pair, the γ parameter with the best fit (lowest RMSE) is selected for each of the five sectors in an iterative approach (Fig. 1). For the regional calibration the summed Antarctic response is the sum of the regionally calibrated contributions with five basin-specific γ values. In addition, the calibration is performed with the same γ value in each region, resulting in Antarctic-wide calibrated γ values.

3 Results

3.1 Basal melt computation and calibration

Basal melt is computed from subsurface ocean temperature time series (Fig. 1). The temperature time series are shown in Figures 3 and 4 for the historical and future period, respectively. Over the 21st century, all regions show a median warming but the magnitude varies between individual regions and becomes scenario dependent around year 2050 (Fig. 4).

The basal melt parameterisations are calibrated by fitting the sea level response of each ESM-RF pair on the Rignot ice discharge time series over the full 1979-2017 period. This exercise shows that the median γ parameter value resulting in the lowest RMSE varies between individual regions (Fig. 5). For the Ross and Weddell regions, a relatively low γ gives a better fit with Rignot data, while for the Amundsen and Peninsula regions a higher γ improves the calibration. The EAIS and Antarctic-

https://doi.org/10.5194/tc-2021-348
Preprint. Discussion started: 24 November 2021


The Cryosphere Discussions
Open Access
EGU

wide calibration give intermediate γ values. The relative magnitudes of the γ values are consistent with the sensitivity to ocean warming of the respective regions as described in Dinniman et al. (2016). For regions with a non-zero contribution to sea level over the observational period, the percentage of greater-than-zero calibrated γ values indicates the percentage of ESM-RF pairs that could be calibrated. For each calibration region, the percentage of ESM-RF pairs with greater-than-zero calibrated γ values (> 0 m yr^{-1}) are therefore indicated in Fig. 5. These percentages show that for most calibration regions, the quadratic parameterisation has a higher percentage of positive values than the linear parameterisation. The boxplots only represent the ESM-RF pairs with positive γ values as indicated by the percentages on top. These percentages show that for the Weddell, Ross and Peninsula sectors less than half of the ESM-RF pairs have greater-than-zero γ values. The calibrated γ values are used in the hindcasts and projections of Antarctic ice discharge.

For the linear parameterisation, we made a comparison between our positive γ values (calibrated on ice discharge) and the γ values used in LARMIP-2 (Levermann et al., 2020) (green shading in Fig. 5, calibrated on basal melt). This comparison shows that our Antarctic-wide calibration results in a median γ just below the lower bound of the Levermann et al. γ range. The same applies to the EAIS sector. For the Amundsen and Peninsula sectors, regional calibration results in γ values at the high end or above the Levermann et al. γ range, while the values for the Ross and Weddell Sea are lower.

For the quadratic parameterisation, a similar comparison was made with the γ values applied in ISMIP6 (Jourdain et al., 2020). Also for the quadratic paramerisation, our median Antarctic-wide calibrated γ (calibrated on four decades of observed ice discharge) sits at the lower end of the γ range of the Antarctic mean calibration (blue shading in Fig. 5, calibrated on basal melt) in ISMIP6. The median EAIS, Ross and Weddell sectors are (just) below the Antarctic mean ISMIP6 range, whereas the Amundsen calibration results in a calibrated median γ at the high end of the Antarctic mean range and the Peninsula calibration gives a median γ just above the Antarctic mean range. In ISMIP6, also a calibration on the Pine Island Glacier basal melt was applied (yellow shading in Fig. 5), which is the highest observed basal melt of the Antarctic ice sheet. Only some of the calibrations of ESM-RF pairs resulted in γ values in the Pine Island Glacier range. However, it should be remarked that the ISMIP6 Pine Island Glacier calibration goes together with negative ocean temperature corrections all around Antarctica that counter-balance the effects of the large γ values.

To summarise, a comparison of the γ values in our study and γ equivalents in LARMIP-2 (Levermann et al., 2020) and ISMIP6 (Jourdain et al., 2020) suggests that calibration on past ice discharge rather than on basal melt observations results in relatively low γ values for the Antarctic-wide calibration. The Amundsen and Peninsula sector are more consistent with the high end of the γ ranges applied in LARMIP-2 and the Antarctic mean calibration of ISMIP6, while the other sectors (EAIS, Ross, Amundsen) are more consistent with the lower end of those γ ranges.

3.2 Hindcasts of Antarctic sea level contribution

Hindcasts of the Antarctic dynamic contribution to sea level rise are made to assess how well Rignot ice discharge could be reproduced after calibration over the period 1979-2017. The total Antarctic sea level response is based on the summed contribution over the five sectors using the six calibrated basal melt computation methods (Table 3).

https://doi.org/10.5194/tc-2021-348
Preprint. Discussion started: 24 November 2021

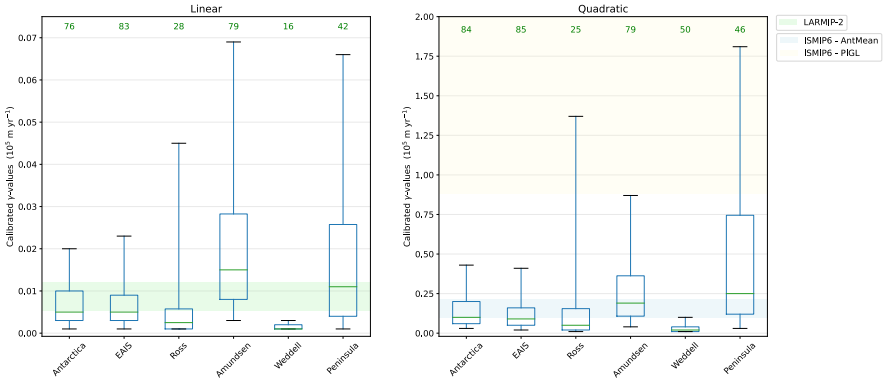

Figure 5. Box-and-whisker plots of calibrated γ values of ESM-RF pairs. Only calibrated γ values greater than zero are shown in the plot. The percentage of ESM-RF pairs with positive γ values is indicated by the green values on top for each region. The horizontal green line indicates the median value, boxes indicate the 25-75 percentile range and whiskers the 5-95 percentile range. Values beyond this range are not shown. The shaded regions indicate γ ranges that are used in other studies. The green shading represents the γ values corresponding with the basal melt sensitivity range of 7-16 m yr^{-1} K^{-1} used in Levermann et al. (2020). The blue and yellow shading indicate the 5-95% range of the γ values used for the nonlocal quadratic parameterisation in ISMIP6 (Jourdain et al., 2020) for both the Antarctic mean (AntMean) and Pine Island Glacier (PIGL) calibration, respectively. For PIGL the 95% bound is 4.71×10^5, which is outside the scale of the vertical axis.

Figure 6 shows the hindcasts of all combinations of CMIP6 models and LARMIP-2 linear response functions using the calibrated γ values (Fig. 5). Each panel represents a basal melt computation method, as specified on top (Table 3). First, we evaluate the magnitude of the modelled sea level contributions. Most ESM-RF pairs are not able to capture the magnitude of the summed Antarctic sea level contribution. For each method, the sea level contribution is underestimated by the median response. This underestimation can be largely attributed to the high number of γ values that were set to zero in the calibration procedure (Sect. 3.1). For the unbounded calibrations (left and middle panels), the sea level response of the multimodel mean value over the 1979-2017 period is approximately half of the magnitude of the observed Antarctic value (Rignot et al., 2019). The median values of the bounded hindcasts (right panels) are closer to observations. This is because the calibrated γ value is greater than zero for each ESM-RF pair. Counter-intuitively at first notice, the linear bounded hindcasts (right panels) have a higher intermodel spread than the unbounded hindcasts. The bounded γ values, however, provide less freedom to restrict the historical response of individual ESM-RF pairs to observations, explaining the higher intermodel spread in the sea level contribution. Hindcasts of regional sea level contributions are further discussed in Appendix A.

https://doi.org/10.5194/tc-2021-348
Preprint. Discussion started: 24 November 2021

3.3 Selection of ESM-RF pairs

From the previous analyses we can conclude that for all basal melt computation methods most ESM-RF pairs are not able to capture the magnitude of the observed Antarctic sea level response to a reasonable extent. This makes them less trustworthy for future projections of the sea level response. Therefore, the calibration on ice discharge is combined with a model selection step in which ESM-RF pairs are selected that capture the summed Antarctic response. ESM-RF pairs are ranked based on their ability to simulate the magnitude of the observed Antarctic ice discharge over the 1979-2017 period. To compare the performance between the different methods, for each method the top 10% best-ranking ESM-RF pairs are selected. By taking the top 10%, the same number of pairs (22) is selected for each method. The best models are defined as the ESM-RF combinations with the lowest RMSE compared to observed ice discharge over the full period. Figure 7 depicts the mean annual sea level contribution biases for this selection of ESM-RF pairs compared to the observations. The mean RMSE over the top 10% ESM-RF pairs is indicated in the legend and the inter-model spread is visualised for the best (QUA, lowest mean RMSE) and worst (LBR, highest mean RMSE) methods. The names of the top 10% ESM-RF combinations for the best method (QUA) are listed in Table A1. The LBR method has the highest mean RMSE due to the wide spread between individual model combinations as explained in Sect. 3.2.

Although the model selection reproduces the summed Antarctic sea level response quite accurately, the acceleration in the observations is not well simulated (Fig. 7). On average, the selected models overestimate Antarctic discharge before around 2010 and underestimate it thereafter. Furthermore, for individual regions the response is not always well captured (see e.g. Figures A1 and A2 for the QUA and QUR method, respectively). The spread in individual regions is higher for the Antarctic-wide calibration than for the regional calibration. Antarctic-wide calibration leads to regional responses that are overestimated in some regions and underestimated in others (Fig. A1) since the same γ is used for each region. Differences between Antarctic-wide and regional calibration are greatest for the Amundsen region, which is the most important contributing region to the summed Antarctic response over the hindcasting period. The Amundsen and Peninsula contributions are underestimated by the selected models for the Antarctic-wide calibration. The EAIS response is reasonably well reproduced. The responses of the Ross and Weddell region are slightly overestimated. The errors in the individual regions compensate each other, resulting in a summed Antarctic response that is well captured. For the regional calibration, the responses in individual regions are better captured and more restricted (Fig. A2).

3.4 Projections

In this section, projections of the summed Antarctic sea level contribution are presented. The projections comprise the 21st century. Computations start in the year 1850 so that the delayed contribution of basal melt is included in the future sea level response. We assess two metrics: the cumulative magnitude and the rate of the sea level response. The cumulative magnitude of the sea level response is used to compare differences over the 21st century. The sea level response rate at the end of the 21st century is indicative of differences in committed sea level rise beyond 2100.

https://doi.org/10.5194/tc-2021-348
Preprint. Discussion started: 24 November 2021

The Cryosphere Discussions
Open Access
EGU

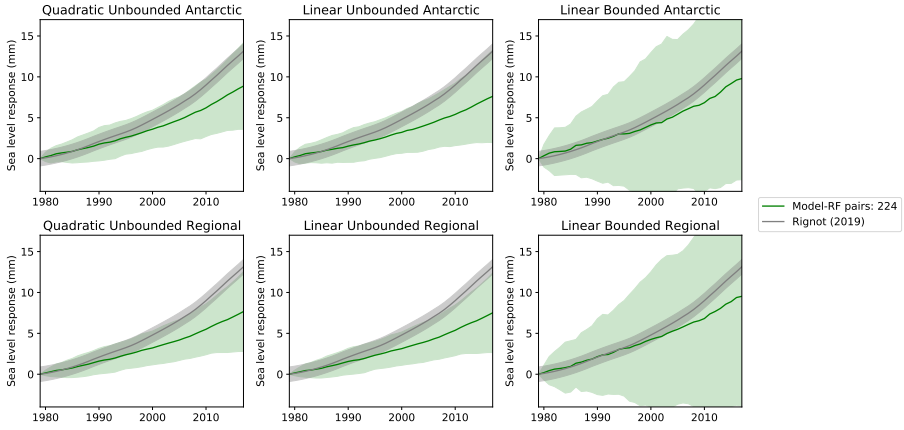

Figure 6. Hindcasts of CMIP6-forced sea level response over the period 1979-2017 based on 14 CMIP6 models and 16 linear response functions. The historical experiment is extended with SSP2-4.5 scenario for the years 2015-2017. The figure shows the results for the full model suite of ESM-RF pairs (green), together with the Rignot ice discharge (grey). The shaded area indicates one standard deviation, representing intermodel spread for the modelled response and observational error for the Rignot data.

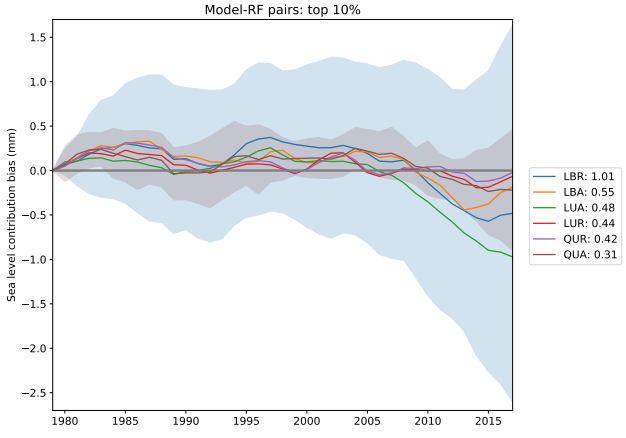

Figure 7. Mean sea level contribution bias compared to observations of the top 10% ESM-RF pairs for each basal melt computation method. The numbers in the legend indicate the mean RMSE over the selected ESM-RF pairs over the period 1979-2017 in mm. The spread (standard deviation) of the top 10% models is indicated for the LBR (highest mean RMSE) and QUA (lowest mean RMSE) methods by the shading in the background.

3.4.1 Magnitude and rate

First, the cumulative magnitude of the sea level response is analysed. The cumulative sea level response is computed by taking the difference between the year 2100 and the average over the period 1995-2014. Figure 8 shows the projected sea level response for each SSP scenario and basal melt computation method. The top panels represent the projections including all

https://doi.org/10.5194/tc-2021-348
Preprint. Discussion started: 24 November 2021

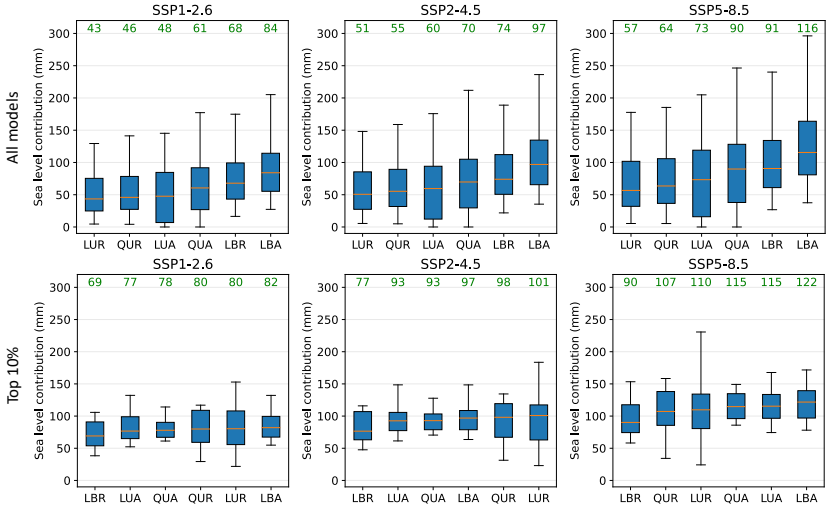

Figure 8. Projected Antarctic sea level response for SSP1-2.6, SSP2-4.5 and SSP5-8.5 in 2100 compared to the period 1995-2005. The spread is determined by the CMIP6 forcing and the LARMIP-2 linear response functions. The top panels show all ESM-RF combinations and the bottom panels the top 10% combinations. The green numbers indicate the median values (the orange lines), whereas the boxes show the 25-75 percentiles and the whiskers the 5-95 percentiles. The basal melt computation methods are ordered from the lowest to the highest median sea level response.

ESM-RF combinations and the bottom panels the top 10% selections. Not surprisingly a higher emission scenerio leads to a higher sea level contribution. Absolute differences between the basal melt computation methods become more explicit for the higher emission scenarios, but relative differences (ratio of highest to lowest) are comparable. For the full model suite, the basal melt computation method affects the relative uncertainty in median sea level contribution more than the SSP scenarios (Table 5).

When the calibration bounds are not considered (unbounded calibrations only), the impact of the basal melt computation reduces. Then the influence of basal melt computation on variation in projected sea level is similar to the influence of scenarios. The basal melt computation can be subdivided into calibration and parameterisation steps. The calibration step is the most distinctive feature of the basal melt computation in terms of the projected magnitude of the sea level contribution. Antarctic-wide calibration results in higher projections than regional calibration. Bounded calibration gives higher values than unbounded calibration (comparison for the linear parameterisation only). The effect of the parameterisation is smallest (comparison for the unbounded calibration only).

Second, the variation in the response rates is assessed at the end of the 21st century (Table 6). These are important for sea level differences beyond 2100. The response rate is computed by a linear regression on the sea level response over the period 2081-2100. The difference between the lowest and highest basal melt method shows that the influence of the basal melt computation method on the response rate is equal to or greater than the effect of the emission scenario. By considering unbounded calibration methods only, the influence of the scenarios dominates over the basal melt computation method. The basal melt

https://doi.org/10.5194/tc-2021-348
Preprint. Discussion started: 24 November 2021

The Cryosphere Discussions
Open Access
EGU

Table 5. Relative uncertainty in the dynamic Antarctic contribution to sea level rise in 2100 compared to 1995-2014. Relative differences were assessed by the variation factor, which is specified as the sea level contribution associated with variations in a specific source variable. If the source variable varies from value A to value B, we quantify the impact of this variable on the sea level contribution by the variation factor B/A (following Hinkel et al. 2021). Only median sea level contributions of ESM-RF pairs are considered.

Variable	Condition	Variation in source variable	Variation factor in sea level
Scenario	All	SSP1-2.6 -> SSP5-8.5	1.3-1.5
Scenario	Top 10%	SSP1-2.6 -> SSP5-8.5	1.3-1.5
Basal melt computation	All	Lowest -> Highest	1.9-2.0
Basal melt computation	Top 10%	Lowest -> Highest	1.2-1.4
Basal melt computation	Unbounded calibration	Lowest -> Highest	1.4-1.6
Calibration region	All	Regional -> Antarctic	1.1-1.4
Calibration bounds	All, Linear parameterisation	Unbounded -> Bounded	1.5-1.8
Parameterisation	All, Unbounded calibration	Linear -> Quadratic	1.1-1.3

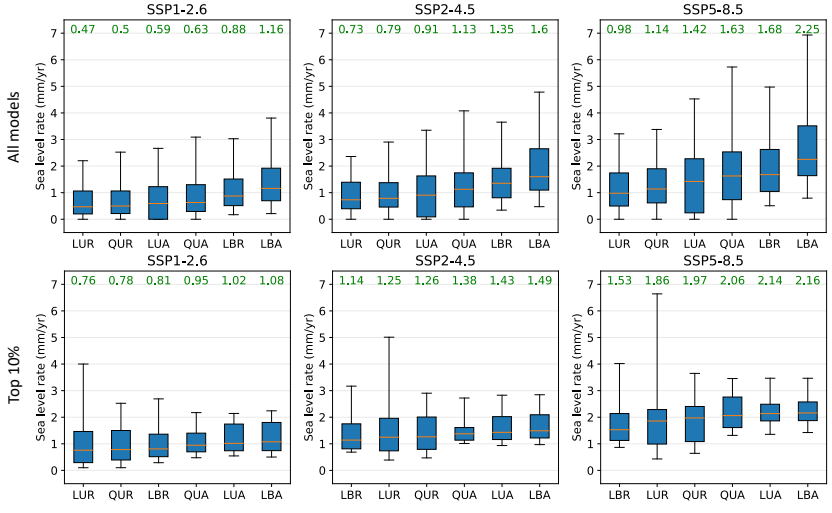

Figure 9. Same as Fig. 8 but for the sea level response rates over the period 2080-2100.

computation can be subdivided into calibration and parameterisation parts. The calibration step is the most distinctive feature in the basal melt computation. Antarctic-wide calibration results in higher projections than regional calibration. Bounded calibration gives higher values than unbounded calibration (comparison for the linear parameterisation only). The effect of the parameterisation is smallest; The quadratic parameterisation provides higher estimates of future sea level rise rates than the linear parameterisation (comparison for the unbounded calibration only).

https://doi.org/10.5194/tc-2021-348
Preprint. Discussion started: 24 November 2021

We conclude that sea level variations associated with basal melt computation methods are equal or greater than variations between different pathways of future greenhouse gas emission scenarios. Within the basal melt computation methods, the calibration step is more important than the parameterisation type for the contribution of Antarctic ice discharge to sea level up to and beyond 2100.

3.4.2 Best estimate

In Sect. 3.3 the top 10% best ESM-RF pairs were selected based on their performance in reproducing observed Antarctic ice discharge over four decades. Figure 10 presents the projections of these selections. For each scenario, the top 10% selection shows on average a 20-28 mm higher median cumulative sea level response than the full model suite (Fig. 8). This can be partly attributed to the fact that the selection does not include models with a γ of zero for the regions that contribute most (Amundsen, EAIS) to the sea level increase. Averaged over all basal melt computation methods, SSP5-8.5 has a median cumulative increase of 110 mm compared to 78 mm in SSP1-2.6. Furthermore, the different basal melt computation methods give more similar results for the selection than for the full model suite (Table 5). In contrast to the full model suite, for the selection there is no clear relation between the basal melt computation method and the response magnitude within an emission scenario. For the top 10% selection the influence on the response magnitude of the basal melt computation method is thus equal to or smaller than the effect of the emission scenario.

The top 10% selection shows on average 0.2-0.5 mm yr^{-1} higher sea level rates than the full model suite (Fig. 9). SSP5-8.5 has a median response rate that is about twice as large as the rate of SSP1-2.6. As for the cumulative contribution, the rates of the selected ESM-RF combinations are more equal between different basal melt computation methods for the model selection than for the full model suite (Table 6). For the top 10% selection the influence on the response rate of the basal melt computation method is smaller than the effect of the emission scenario. Different than for the full model suite, the selection consistently shows higher sea level rates for the Antarctic-wide calibration than for the regional calibration. This can be explained by the higher contributions (higher γ) of the Ross and Weddell sectors, which show a clear warming trend in the subsurface ocean (Fig. 4). Other aspects (bounded vs unbounded calibration, quadratic vs linear parameterization) do not have a noticeable effect on the response rate of the top 10% selection.

For the top 10% of each basal melt computation method, the quadratic parameterisation combined with an Antarctic-wide calibration (QUA) resulted in the best estimate of Antarctic discharge over almost four decades (lowest overall RMSE) (Sect. 3.2). If reproducing the past is good indicator for making future projections, this basal melt computation method (QUA) will arguably provide the best estimate for the sea level contribution of Antarctic discharge over the coming century. We compared our best estimate with the emulated ISMIP6 and LARMIP-2 studies as presented in IPCC AR6 (Table 7). The cumulative sea level response is equal or smaller in magnitude than emulated ISMIP6 estimates across all scenarios (depending on the basal melt computation method). Compared to LARMIP-2, the response is smaller. The differences with ISMIP6 and LARMIP-2 can be mainly attributed to the calibration on past ice discharge, which resulted in less sensitive basal melt parameterisations (Fig. 5).

https://doi.org/10.5194/tc-2021-348
Preprint. Discussion started: 24 November 2021

Table 6. Similar to Table 5, but for the sea level response rate over 2081-2100.

Variable	Condition	Variation in source variable	Variation factor in sea level
Scenario	All	SSP1-2.6 -> SSP5-8.5	1.9-2.6
Scenario	Top 10%	SSP1-2.6 - SSP5-8.5	1.9-2.5
Basal melt computation	All	Lowest -> Highest	2.2-2.5
Basal melt computation	Top 10%	Lowest -> Highest	1.2-1.4
Basal melt computation	Unbounded calibration	Lowest -> Highest	1.3-1.7
Calibration region	All	Regional -> Antarctic	1.2-1.4
Calibration bounds	All, Linear parameterisation	Unbounded -> Bounded	1.6-2.0
Parameterisation	All, Unbounded calibration	Linear -> Quadratic	1.1-1.2

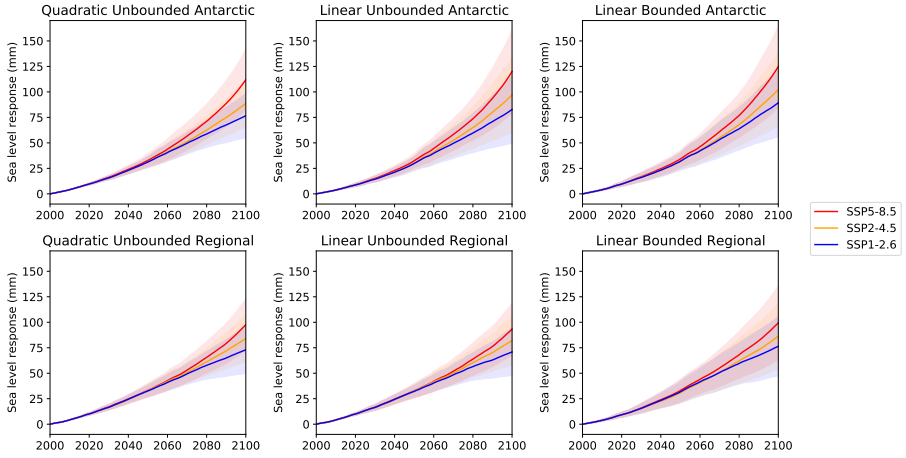

Figure 10. Projections of Antarctic sea level response for SSP1-2.6, SSP2-4.5 and SSP5-8.5 using the top 10% selected ESM-RF combinations. The spread is determined by the CMIP6 forcing and the LARMIP-2 linear response functions.

3.4.3 Modelling uncertainties

Here we assess the role of CMIP6 ESMs and LARMIP-2 ice sheet models in projection uncertainties by comparing the median projected sea level contributions for the basal melt computation method with the best performance in the hindcasts (QUA). Fig. 11 shows the projected Antarctic sea level contribution for each individual CMIP6 model as computed with the QUA method. The spread for each CMIP6 model is determined by the linear response functions. Noticeably, the differences between the scenarios are small compared to the the differences between individual CMIP6 models. The median sea level contribution for SSP1-2.6 (SSP5-8.5) varies from 0 mm (0 mm) for CAS-ESM2-0 to 174 (254) mm for MPI-ESM1-2-LR. This difference can be attributed to the difference between CMIP6 models.

https://doi.org/10.5194/tc-2021-348
Preprint. Discussion started: 24 November 2021

The Cryosphere Discussions
Open Access
EGU

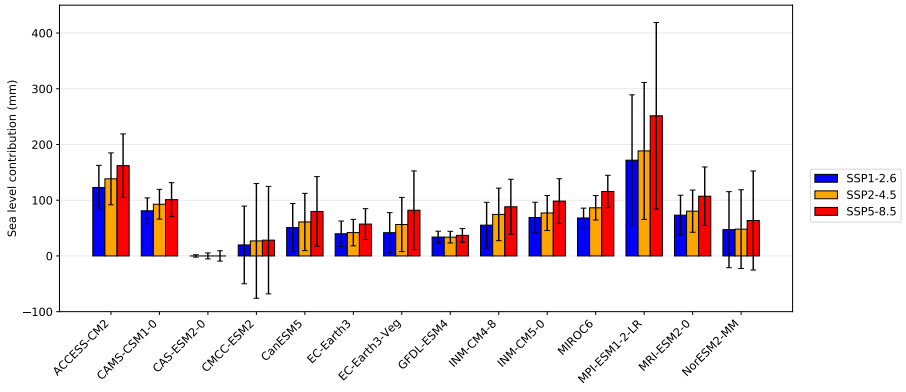

Figure 11. Projected Antarctic sea level changes for SSP1-2.6 (blue), SSP2-4.5 (orange) and SSP5-8.5 (red) over the 21st century, defined as the difference between year 2100 and the period 1995-2014. For each CMIP6 model, the errorbars indicate one standard deviation between the associated RF timeseries. Basal melt is computed with the quadratic parameterisation which is calibrated Antarctic-wide (QUA).

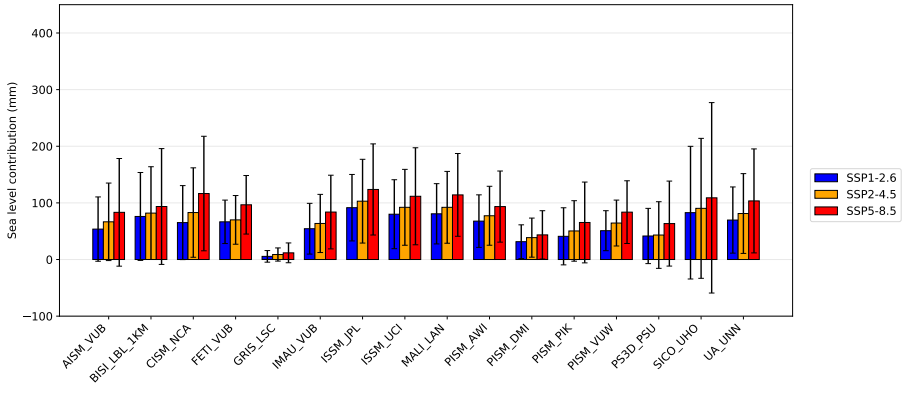

Figure 12. Projected Antarctic sea level changes for SSP1-2.6 (blue), SSP2-4.5 (orange) and SSP5-8.5 (red) over the 21st century, defined as the difference between year 2100 and the period 1995-2014. For each RF, the errorbars indicate one standard deviation between the associated CMIP6 models. Basal melt is computed with the quadratic parameterisation which is calibrated Antarctic-wide (QUA).

Similar to Fig. 11, Fig. 12 shows the projected Antarctic sea level contribution for each individual ice sheet model (RF). Here, the spread is determined by the CMIP6 models. Clearly, the spread between RFs is smaller than between CMIP6 models. Furthermore, the RF spread is also greater than the scenario-induced spread. The sea level contribution for SSP1-2.6 (SSP5-8.5) varies from 6 mm (10 mm) for GRIS-LSC to 86 mm (127 mm) for ISSM-JPL, pointing at a difference that can be attributed to ice sheet models of 80 mm (117) mm, influencing the sea level contribution by a factor 12.7 (14.3).

https://doi.org/10.5194/tc-2021-348
Preprint. Discussion started: 24 November 2021

4 Discussion

In this study, calibrated projections of Antarctica's dynamic sea level contribution were made that are consistent with four decades of past ice discharge in observations. Calibration was applied on the basal melt parameterisation. The contribution of Antarctica's ice discharge to sea level changes is computed with state-of-the-art ESMs from Coupled Model Intercomparison Project Phase 6 (CMIP6) and linear response functions from LARMIP-2 ice sheet models. The major strength of this method is that multiple climate and ice sheet models can be combined to assess the full range of modelling uncertainties. A drawback of the method is that non-linearities between thermal forcing and ice sheet mass loss, related to ice sheet instabilities are not considered because we use the Linear Response Functions framework. Our results show that the models that we used, even the top 10%, are not able to represent the acceleration present in the observations (Fig. 7), with overestimation of mass loss before 2010 and underestimation thereafter. This could be explained by ice sheet/ocean feedbacks that are not represented in the models. One reason to introduce the quadratic parameterisation was to account for some positive feedback between ice melt and ocean forcing. However the feedback between surface freshening due to melt water and basal ice shelf melt is not explicitly simulated. Recent studies suggest that this feedback is positive (Bronselaer et al., 2018; Golledge et al., 2019; Sadai et al., 2020), which could explain the inability of our models to represent the observed acceleration. It should also be noted that our study does not address the impact of surface melt on calving nor marine ice cliff instability processes, which means that the projections are a lower bound of what could happen in reality.

Temperature-melt relations are typically parameterised in terms of the heat exchange velocity γ (Favier et al., 2019). The region of calibration is relevant for the projections, since the calibrated γ value varies around the continent and is dependent on the ice-shelf cavity type. Calibration of the γ value in the basal melt parameterisation results regularly in a value of zero, especially for the Weddell and Ross regions. A γ value of zero indicates insensitivity of basal melt to open ocean subsurface temperature changes. The likeliest explanation would be that the models predict a warming while the observed discharge decreased over the observation period (or vice versa). This could be caused either by the importance of natural variability in the observations or by the inability of the ESMs to simulate temperature trends around Antarctica. Furthermore, the observed ice discharge trend could be close to zero (for the Weddell sector). Another explanation is that the water inside the ice shelf cavities is blocked from the water in the coastal region outside the cavities due to density gradients. This contradicts the assumption in this study that water from the open ocean can freely access the ice shelf cavities. It is questionable whether the situation during the calibration period is representative for the future. In the future model projections (Fig. 4), especially for SSP5-8.5, all coastal regions, especially the Weddell and Ross sectors, experience a warming signal. As the open ocean outside the cavities warms, it could be expected that this warming will at a certain moment also be transported inside the cavities, and contribute there to basal melt and ice discharge. New calibration will then lead to γ values that are greater than zero. This means that calibrated γ values that link open ocean subsurface temperatures outside cavities to basal melt underneath ice shelves could be climate-state dependent. It should also be noted that we calibrated the basal melt parameterisation based on basal melt anomalies and not on absolute basal melt. This is because that allows us to better represent observed melt but the

https://doi.org/10.5194/tc-2021-348
Preprint. Discussion started: 24 November 2021


The Cryosphere Discussions

Table 7. Projected dynamic contributions to sea level in meters from the Antarctic ice sheet in 2100 relative to 1995-2014. The numbers for LARMIP-2, ISMIP6 and SMB are obtained from the IPCC AR6 report (Fox-Kemper et al., 2021). Note that for the ISMIP6 estimate surface mass balance contributions are removed as our study only accounts for ice discharge. QUA and LBA are shown as the best-performing method in reproducing hindcasts (QUA) and the method that is most comparable to the LARMIP-2 experiment, but calibrated on past ice discharge (LBA) (Fig. 7).

Scenario	Forcing/Source	16.6%	50%	83.3%
SSP5-8.5/RCP8.5	Selected models / QUA	0.10	0.12	0.13
	Selected models / LBA	0.10	0.12	0.14
	ISMIP6 excluding SMB	0.10	0.13	0.17
	LARMIP-2	0.10	0.20	0.39
SSP2-4.5/RCP4.5	Selected models / QUA	0.08	0.09	0.10
	Selected models / LBA	0.06	0.10	0.12
	ISMIP6 excluding SMB	0.07	0.12	0.16
	LARMIP-2	0.09	0.17	0.33
SSP1-2.6/RCP2.6	Selected models / QUA	0.07	0.08	0.09
	Selected models / LBA	0.07	0.08	0.10
	ISMIP6 excluding SMB	0.06	0.11	0.15
	LARMIP-2	0.08	0.15	0.29

downside is that anomalies are a second order effect that is harder to model. Lastly, in the current generation of ESMs (CMIP6) ice shelf cavities are not (fully) represented, leading to deficiencies in the process representation (Mathiot et al., 2017).

In this study, an Antarctic-wide and regional calibration of the basal melt parameterisation have been applied. Arguably, the regional parameterisation is more physically correct since individual regions might respond differently to similar forcing due to differences in ice and ocean dynamics and ice geometries. However, for the Ross, Weddell and Peninsula regions, 50-84% of the ESM-RF combinations have a calibrated γ equal to zero, resulting in no sea level contribution in future projections. For these regions, regional calibration leads to lower median contributions than Antarctic-wide calibration. A possible reason is that these regions have no clear ocean temperature trend over the period 1850-2018 (and thus small thermal forcing) and relatively small changes in ice discharge during the calibration period. Calibrating on the Antarctic-wide response gives a less accurate reproduction of the historical mass loss in these regions, but arguably a better prediction of future mass loss (when the ocean is warming in these regions). Also, it should be noted that the quadratic parameterisation does introduce some regional difference in basal melt sensitivity, with a lower sensitivity in colder cavities. Since both calibration methods have their advantages and disadvantages, we applied and compared both calibration methods.

Each basal melt parameterisation method has been calibrated on ice discharge. For two basal melt computation methods (LBA, LBR) additional calibration has been performed on basal melt itself by setting observation-based bounds on the cali-

https://doi.org/10.5194/tc-2021-348
Preprint. Discussion started: 24 November 2021

bration parameter γ. The results show that basal-melt constrained (bounded) projections (LBA, LBR) lead to higher sea level estimates than their unconstrained (unbounded) counterparts (LUA, LUR). The main reason for this is that for the bounded calibration γ values are greater than zero for all ESM-RF pairs, whereas for the unbounded calibration only 16-85% of the ESM-RF pairs have values greater than zero (Fig. 5). Parameter constraints on the heat exchange velocity γ in the bounded calibrations were obtained from the basal melt sensitivity parameter from the Levermann et al. (2020) range of 7-16 m yr^{-1} K^{-1}. Therefore it is interesting to compare the sea level contribution projections of the linear bounded Antarctic (LBA) calibration method with the LARMIP-2 projections over the same period (as presented in IPCC AR6). The Antarctic-wide calibration is compared since LARMIP-2 also applies the same basal melt sensitivity in each region. In LARMIP-2 the median projected sea level contribution is 0.15 m for RCP2.6 and 0.20 m for RCP8.5, compared to 0.08 m for SSP1-2.6 and 0.12 m for SSP5-8.5 in our study. The calibrated basal melt sensitivity (based on the associated calibrated γ value, Fig. 5) in our study has a median value of 7 m yr^{-1} K^{-1} for all calibration regions, except for the Amundsen sector, which has a median basal melt sensitivity of 12 m yr^{-1} K^{-1}. Also, Antarctic-wide calibration resulted in a median γ of 7 m yr^{-1} K^{-1}, this is the lower bound of the basal melt sensitivity range. Note that these values are different than the medians in Fig. 5 since here all ESM-RF pairs are included (as they all have positive values by definition) while Fig. 5 only includes a percentage of the models (those with positive γ values). This means that the randomly drawn γ values from the full range in the Levermann et al. study result on average in a more sensitive basal melt parameterisation than the calibrated γ values in our study and suggests that their basal melt sensitivity range should be revised downward to be consistent with past ice discharge. Here, it should also be noted that LARMIP-2 overestimates the mass loss observations of Shepherd et al. (2018). The same argument applies to the ISMIP6 γ-values. Similar to LARMIP-2, calibration shows that γ values in the lower bound of the Antarctic mean range applied in ISMIP6 are more consistent with four decades of past Antarctic ice discharge (Fig. 5). Consistent with the higher melt sensitivity the projected sea level contributions are therefore higher in LARMIP-2 and ISMIP6.

A short assessment was made on the role of CMIP6 ESMs and LARMIP-2 ice sheet models in projection uncertainties by comparing the median projected sea level contributions for the basal melt computation method with the best performance in the hindcasts (QUA) (Sect. 3.4.3). This assessment shows that modelling uncertainties, especially those related to ocean temperature evolution from ESMs, are a greater source of uncertainty in Antarctic mass loss projections than the emission scenarios and the basal melt computation method. These large intermodel differences in ESMs as well as RFs explain why model selection is essential to make future projections more consistent with observations of past ice discharge.

5 Conclusions

This study presents calibrated projections of Antarctica's ice discharge in 2100 compared to present-day (1995-2014). Ocean thermal forcing is based on regional subsurface ocean temperature from 14 CMIP6 ESMs and 3 SSP scenarios and bias-adjusted with GREP ocean reanalysis data. Basal melt is computed with a linear and quadratic relation with ocean thermal forcing. The ice discharge is calculated with 16 linear response functions (RF) based on ice sheet model experiments from LARMIP-2. New compared to other studies is the calibration of the modelled response. We applied a different, iterative

https://doi.org/10.5194/tc-2021-348
Preprint. Discussion started: 24 November 2021

approach to calibrate the basal melt computation (Fig. 1) since there is still high uncertainty in the temperature-basal melt relation (Dinniman et al., 2016). Past observations of ice discharge rather than basal melt are used for calibration of the melt parameterisation. The calibrated γ value for each individual ESM-RF pair is the one that is most consistent with four decades of observed ice discharge (Rignot et al., 2019). Apart from the bounded calibrations, the only (physical) limitation is that γ should be greater or equal to zero. Finally a top 10% selection of ESM-RF combinations is made, based on their performance in reproducing past ice discharge.

The projected Antarctic discharge shows a clear sensitivity to the emission scenario. Limiting emissions to scenario SSP1-2.6 compared to SSP5-8.5, would lead to about 30% reduction in the median projected sea level contribution of Antarctic discharge in 2100. The delayed feedback of ice discharge to increasing ocean temperatures (as modelled by the linear response functions) implies that the associated sea level contribution only becomes scenario-dependent after around 2050.

For the full model suite, the basal melt computation method has a greater impact on the projected sea level contribution than the emission scenario. Across all scenarios, the median Antarctic ice loss is two times higher for the highest method than for the lowest method. Bounded calibration leads to higher median projections than unbounded calibration since all γ values are greater than zero due to the lower bound. Calibrating on the summed Antarctic response leads to higher projections than calibration per region. This can be explained by regions with a small or negative past contribution to sea level that have calibrated regional γ values equal to zero (Ross, Weddell), and therefore have no contribution in future projections even if the subsurface ocean is warming. Adapting Antarctic-wide γ values results in a positive value and positive future contribution for these regions. The basal melt parameterisation (quadratic or linear) is least important for the projections.

The top 10% selection gives 20-28 mm higher median projections than the full model suite. This difference can be partly attributed to the unbounded basal melt computation methods, which include γ values equal to zero for the full model suite. After selection, the top 10% γ values are greater than zero for the dominant contributing regions (Amundsen, EAIS), resulting in higher estimates. For the bounded methods, there is no significant difference between the full model selection and top 10%.

This study shows that calibration of the basal melt parameterisation on past ice discharge provides a way to constrain historical and future evolution of Antarctic basal melt to observations. This leads to reduced spread in the projections of the sea level contribution of Antarctica's ice discharge from basal melt over the 21st century. Moreover, this calibration shows that the two main studies on which the IPCC AR6 Antarctic sea level contributions are based (ISMIP6 and LARMIP-2) use basal melt sensitivities that are higher than the calibrated values that we found. If these studies would have calibrated their basal melt computations on past observations of ice discharge, this would have resulted in lower projections of Antarctica's sea level contribution.

6 Code and data availability

– Linear response functions from LARMIP-2 (Levermann et al., 2020): https://github.com/ALevermann/Larmip2020/tree/master/RFunctions

https://doi.org/10.5194/tc-2021-348
Preprint. Discussion started: 24 November 2021

- Global ocean reanalyses: https://resources.marine.copernicus.eu/?option=com_csw&view=details&product_id=GLOBAL_REANALYSIS_PHY_001_026
- Antarctic ice discharge (Rignot et al., 2019): https://www.pnas.org/highwire/filestream/844425/field_highwire_adjunct_files/1/pnas.1812883116.sd01.xlsx

Appendix A: Hindcasts of regional sea level contributions

Figures A1 and A2 show the regional sea level contributions of the top 10% best-performing models of the quadratic parameterisation for the Antarctic-wide and regional calibration, respectively. Especially for the Weddell region, the quadratic parameterisation can be better calibrated on the observations (50% positive γ values) than the linear parameterisation (16%). This is due to the parabolic shape of the observed ice discharge over the observational period (Fig. A2). For the Weddell region, the cumulative ice discharge is close to zero, resulting in the relatively small calibrated γ values. For the Ross region, the Rignot ice discharge even shows a declining sea level contribution over the reanalysis period, which could not even be reproduced by the best fitting CMIP6 models (Fig. A2). Figure 3 consistently shows no decline in the median ocean temperature of the CMIP6 models over the historical period, pointing at a deficiency in ocean forcing for the Ross region. In the Ross region negative γ values would give a better fit for many ESM-RF pairs, but this would be physically incorrect since this would suggest that warmer temperatures lead to less basal melt and vice versa. As a consequence, a high percentage of the ESM-RF pairs has a γ with a value of zero in the Ross region. For the Peninsula, about half of the models has a γ value of zero. Consistently, most CMIP6 models do not simulate a positive temperature trend in this region over the historical period (Fig. 3), also pointing at a deficiency in the ocean forcing. For the Amundsen and EAIS regions, most models have positive calibrated γ values, consistent with the positive sea level contribution in these regions and simulated ocean warming trend over the historical period.

Author contributions. EvdL, SD and DLB designed the study. DLB downloaded the CMIP6 data from the ESGF node and wrote the code to read it. EvdL performed the computations and prepared the manuscript with contributions from all co-authors.

Competing interests. The authors declare that they have no conflict of interest.

https://doi.org/10.5194/tc-2021-348
Preprint. Discussion started: 24 November 2021

The Cryosphere Discussions
Open Access
EGU

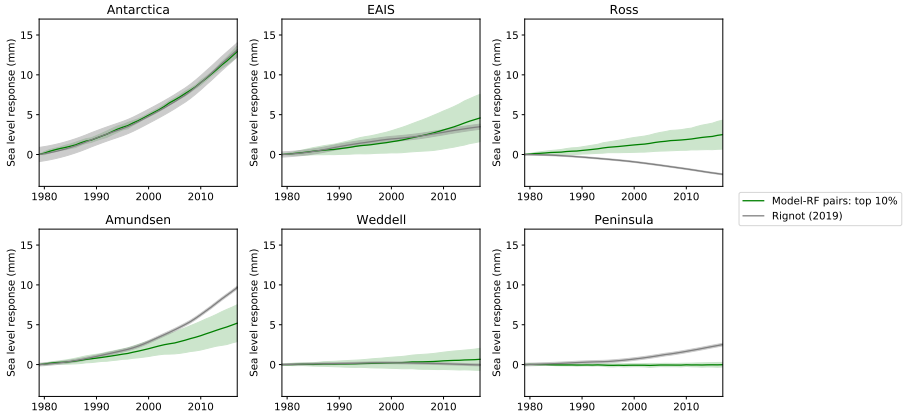

Figure A1. Regional hindcasts of the top 10% ESM-RF pairs for the QUA method over the period 1979-2017 (Table A1). The historical experiment is extended with SSP2-4.5 scenario for the years 2015-2017. The figure shows the results for the top 10% ESM-RF pairs (green), together with the Rignot ice discharge (grey). The shaded area indicates one standard deviation, representing intermodel spread for the modelled response and observational error for the Rignot data.

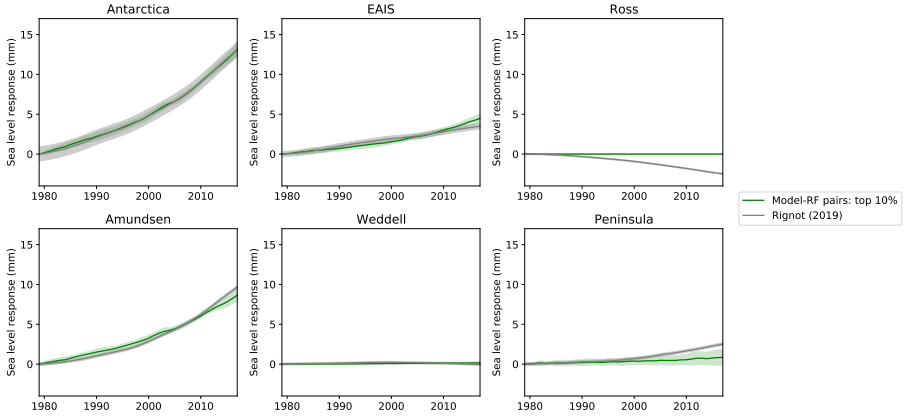

Figure A2. Same as Fig. A1, but for the QUR method.

References

Bamber, J. L. and Aspinall, W. P.: An expert judgement assessment of future sea level rise from the ice sheets, Nature Climate Change, 3, 424–427, https://doi.org/10.1038/nclimate1778, 2013.

Bamber, J. L., Oppenheimer, M., Kopp, R. E., Aspinall, W. P., and Cooke, R. M.: Ice sheet contributions to future sea-level rise from structured expert judgment, Proceedings of the National Academy of Sciences of the United States of America, 166, 11 195–11 200, https://doi.org/10.1073/pnas.1817205116, 2019.

https://doi.org/10.5194/tc-2021-348
Preprint. Discussion started: 24 November 2021


The Cryosphere Discussions
Open Access
EGU

Table A1. Top 10% model pairs of the quadratic parameterisation with Antarctic-wide calibration (QUA).

Earth system model	Ice sheet model
INM-CM5-0	MALI LAN
INM-CM4-8	MALI LAN
EC-Earth3	ISSM JPL
CAMS-CSM1-0	SICO UHO
MIROC6	UA UNN
INM-CM4-8	UA UNN
MIROC6	ISSM UCI
EC-Earth3	IMAU VUB
INM-CM4-8	AISM VUB
MRI-ESM2-0	CISM NCA
CAMS-CSM1-0	MALI LAN
MIROC6	AISM VUB
MIROC6	CISM NCA
MRI-ESM2-0	MALI LAN
INM-CM5-0	ISSM JPL
ACCESS-CM2	AISM VUB
CAMS-CSM1-0	CISM NCA
MRI-ESM2-0	BISI LBL 1KM
CanESM5	CISM NCA
MRI-ESM2-0	SICO UHO
MRI-ESM2-0	ISSM JPL
CAMS-CSM1-0	UA UNN

Barthel, A., Agosta, C., Little, C. M., Hattermann, T., Jourdain, N. N., Goelzer, H., Nowicki, S., Seroussi, H., Straneo, F., and Bracegirdle, T. T.: CMIP5 model selection for ISMIP6 ice sheet model forcing: Greenland and Antarctica, Cryosphere, 14, 855–879, https://doi.org/10.5194/tc-14-855-2020, 2020.

Bronselaer, B., Winton, M., Griffies, S. M., Hurlin, W. J., Rodgers, K. B., Sergienko, O. V., Stouffer, R. J., and Russell, J. L.: Change in future climate due to Antarctic meltwater, Nature, 564, 53–58, https://doi.org/10.1038/s41586-018-0712-z, 2018.

Clark, P. U., Shakun, J. D., Marcott, S. A., Mix, A. C., Eby, M., Kulp, S., Levermann, A., Milne, G. A., Pfister, P. L., Santer, B. D., Schrag, D. P., Solomon, S., Stocker, T. F., Strauss, B. H., Weaver, A. J., Winkelmann, R., Archer, D., Bard, E., Goldner, A., Lambeck, K., Pierrehumbert, R. T., and Plattner, G. K.: Consequences of twenty-first-century policy for multi-millennial climate and sea-level change, Nature Climate Change, 6, 360–369, https://doi.org/10.1038/nclimate2923, 2016.

Dangendorf, S., Hay, C., Calafat, F. M., Marcos, M., Piecuch, C. G., Berk, K., and Jensen, J.: Persistent acceleration in global sea-level rise since the 1960s, Nature Climate Change, 9, 705–710, https://doi.org/10.1038/s41558-019-0531-8, http://dx.doi.org/10.1038/s41558-019-0531-8http://www.nature.com/articles/s41558-019-0531-8, 2019.

DeConto, R. M. and Pollard, D.: Contribution of Antarctica to past and future sea-level rise, Nature, 531, 591–597, https://doi.org/10.1038/nature17145, http://dx.doi.org/10.1038/nature17145, 2016.

Dinniman, M. S., Asay-Davis, X. S., Galton-Fenzi, B. K., Holland, P. R., Jenkins, A., and Timmermann, R.: Modeling ice shelf/ocean interaction in Antarctica: A review, Oceanography, 29, 144–153, https://doi.org/10.5670/oceanog.2016.106, 2016.

Edwards, T. L., Nowicki, S., Marzeion, B., Hock, R., Goelzer, H., Seroussi, H., Jourdain, N. C., Slater, D. A., Turner, F. E., Smith, C. J., McKenna, C. M., Simon, E., Abe-Ouchi, A., Gregory, J. M., Larour, E., Lipscomb, W. H., Payne, A. J., Shepherd, A., Agosta, C., Alexander, P., Albrecht, T., Anderson, B., Asay-Davis, X., Aschwanden, A., Barthel, A., Bliss, A., Calov, R., Chambers, C., Champollion, N., Choi, Y., Cullather, R., Cuzzone, J., Dumas, C., Felikson, D., Fettweis, X., Fujita, K., Galton-Fenzi, B. K., Gladstone, R., Golledge, N. R., Greve, R., Hattermann, T., Hoffman, M. J., Humbert, A., Huss, M., Huybrechts, P., Immerzeel, W., Kleiner, T., Kraaijenbrink, P., Le clec'h, S., Lee, V., Leguy, G. R., Little, C. M., Lowry, D. P., Malles, J. H., Martin, D. F., Maussion, F., Morlighem, M., O'Neill, J. F., Nias, I., Pattyn, F., Pelle, T., Price, S. F., Quiquet, A., Radić, V., Reese, R., Rounce, D. R., Rückamp, M., Sakai, A., Shafer, C., Schlegel, N. J., Shannon, S., Smith, R. S., Straneo, F., Sun, S., Tarasov, L., Trusel, L. D., Van Breedam, J., van de Wal, R., van den Broeke, M., Winkelmann, R., Zekollari, H., Zhao, C., Zhang, T., and Zwinger, T.: Projected land ice contributions to twenty-first-century sea level rise, Nature, 593, 74–82, https://doi.org/10.1038/s41586-021-03302-y, 2021.

Eyring, V., Bony, S., Meehl, G. A., Senior, C. A., Stevens, B., Stouffer, R. J., and Taylor, K. E.: Overview of the Coupled Model Intercomparison Project Phase 6 (CMIP6) experimental design and organization, Geoscientific Model Development, 9, 1937–1958, https://doi.org/10.5194/gmd-9-1937-2016, 2016.

Favier, L., Jourdain, N. C., Jenkins, A., Merino, N., Durand, G., Gagliardini, O., Gillet-Chaulet, F., and Mathiot, P.: Assessment of Sub-Shelf Melting Parameterisations Using theOcean-Ice Sheet Coupled Model NEMO(v3.6)-Elmer/Ice(v8.3), Geoscientific Model Development Discussions, pp. 1–40, https://doi.org/10.5194/gmd-2019-26, 2019.

Fox-Kemper, B., H. T. Hewitt, C. Xiao, G. Aðalgeirsdóttir, S. S. Drijfhout, T. L. Edwards, N. R. Golledge, M. Hemer, R. E. Kopp, G. Krinner, A. Mix, D. Notz, S. Nowicki, I. S. Nurhati, L. Ruiz, Sallée, J.-B., Slangen, A. B. A., and Yu, Y.: Ocean, Cryosphere and Sea Level Change, Tech. rep., 2021.

Golledge, N. R., Keller, E. D., Gomez, N., Naughten, K. A., Bernales, J., Trusel, L. D., and Edwards, T. L.: Global environmental consequences of twenty-first-century ice-sheet melt, Nature, 566, 65–72, https://doi.org/10.1038/s41586-019-0889-9, http://dx.doi.org/10.1038/s41586-019-0889-9, 2019.

Haasnoot, M., Kwadijk, J., Van Alphen, J., Le Bars, D., Van Den Hurk, B., Diermanse, F., Van Der Spek, A., Oude Essink, G., Delsman, J., and Mens, M.: Adaptation to uncertain sea-level rise; how uncertainty in Antarctic mass-loss impacts the coastal adaptation strategy of the Netherlands, Environmental Research Letters, 15, https://doi.org/10.1088/1748-9326/ab666c, 2020.

Hinkel, J., Lincke, D., Vafeidis, A. T., Perrette, M., Nicholls, R. J., Tol, R. S., Marzeion, B., Fettweis, X., Ionescu, C., and Levermann, A.: Coastal flood damage and adaptation costs under 21st century sea-level rise, Proceedings of the National Academy of Sciences of the United States of America, 111, 3292–3297, https://doi.org/10.1073/pnas.1222469111, 2014.

Hinkel, J., Feyen, L., Hemer, M., Cozannet, G., Lincke, D., Marcos, M., Mentaschi, L., Merkens, J. L., Moel, H., Muis, S., Nicholls, R. J., Vafeidis, A. T., Wal, R. S. W., Vousdoukas, M. I., Wahl, T., Ward, P. J., and Wolff, C.: Uncertainty and Bias in Global to Regional Scale Assessments of Current and Future Coastal Flood Risk, Earth's Future, 9, https://doi.org/10.1029/2020ef001882, 2021.

https://doi.org/10.5194/tc-2021-348
Preprint. Discussion started: 24 November 2021

Jenkins, A., Shoosmith, D., Dutrieux, P., Jacobs, S., Kim, T. W., Lee, S. H., Ha, H. K., and Stammerjohn, S.: West Antarctic Ice Sheet retreat in the Amundsen Sea driven by decadal oceanic variability, Nature Geoscience, 11, 733–738, https://doi.org/10.1038/s41561-018-0207-4, http://dx.doi.org/10.1038/s41561-018-0207-4, 2018.

Jourdain, N. C., Asay-Davis, X., Hattermann, T., Straneo, F., Seroussi, H., Little, C. M., and Nowicki, S.: A protocol for calculating basal melt rates in the ISMIP6 Antarctic ice sheet projections, The Cryosphere, 14, 3111–3134, https://doi.org/10.5194/tc-14-3111-2020, https://tc.copernicus.org/articles/14/3111/2020/, 2020.

Lambert, E., Le Bars, D., Goelzer, H., and van de Wal, R. S.: Correlations Between Sea-Level Components Are Driven by Regional Climate Change, Earth's Future, 9, 1–17, https://doi.org/10.1029/2020EF001825, 2021.

Levermann, A., Winkelmann, R., Nowicki, S., Fastook, J. L., Frieler, K., Greve, R., Hellmer, H. H., Martin, M. A., Meinshausen, M., Mengel, M., Payne, A. J., Pollard, D., Sato, T., Timmermann, R., Wang, W. L., and Bindschadler, R. A.: Projecting Antarctic ice discharge using response functions from SeaRISE ice-sheet models, Earth System Dynamics, 5, 271–293, https://doi.org/10.5194/esd-5-271-2014, 2014.

Levermann, A., Winkelmann, R., Albrecht, T., Goelzer, H., Golledge, N. R., Greve, R., Huybrechts, P., Jordan, J., Leguy, G., Martin, D., Morlighem, M., Pattyn, F., Pollard, D., Quiquet, A., Rodehacke, C., Seroussi, H., Sutter, J., Zhang, T., Van Breedam, J., Calov, R., Deconto, R., Dumas, C., Garbe, J., Hilmar Gudmundsson, G., Hoffman, M. J., Humbert, A., Kleiner, T., Lipscomb, W. H., Meinshausen, M., Ng, E., Nowicki, S. M., Perego, M., Price, S. F., Saito, F., Schlegel, N. J., Sun, S., and Van De Wal, R. S.: Projecting Antarctica's contribution to future sea level rise from basal ice shelf melt using linear response functions of 16 ice sheet models (LARMIP-2), Earth System Dynamics, 11, 35–76, https://doi.org/10.5194/esd-11-35-2020, 2020.

Little, C. M. and Urban, N. M.: CMIP5 temperature biases and 21st century warming around the Antarctic coast, Annals of Glaciology, 57, 69–78, https://doi.org/10.1017/aog.2016.25, 2016.

Liu, Y., Moore, J. C., Cheng, X., Gladstone, R. M., Bassis, J. N., Liu, H., Wen, J., and Hui, F.: Ocean-driven thinning enhances iceberg calving and retreat of Antarctic ice shelves, Proceedings of the National Academy of Sciences of the United States of America, 112, 3263–3268, https://doi.org/10.1073/pnas.1415137112, 2015.

Mathiot, P., Jenkins, A., Harris, C., and Madec, G.: Explicit representation and parametrised impacts of under ice shelf seas in the z_*-coordinate ocean model NEMO 3.6, Geoscientific Model Development, 10, 2849–2874, https://doi.org/10.5194/gmd-10-2849-2017, 2017.

Nerem, R. S., Beckley, B. D., Fasullo, J. T., Hamlington, B. D., Masters, D., and Mitchum, G. T.: Climate-change–driven accelerated sea-level rise detected in the altimeter era, Proceedings of the National Academy of Sciences of the United States of America, 115, 2022–2025, https://doi.org/10.1073/pnas.1717312115, 2018.

Nowicki, S., Goelzer, H., Seroussi, H., Payne, A. J., Lipscomb, W. H., Abe-Ouchi, A., Agosta, C., Alexander, P., Asay-Davis, X. S., Barthel, A., Bracegirdle, T. J., Cullather, R., Felikson, D., Fettweis, X., Gregory, J. M., Hattermann, T., Jourdain, N. C., Kuipers Munneke, P., Larour, E., Little, C. M., Morlighem, M., Nias, I., Shepherd, A., Simon, E., Slater, D., Smith, R. S., Straneo, F., Trusel, L. D., Van Den Broeke, M. R., and Van De Wal, R.: Experimental protocol for sea level projections from ISMIP6 stand-alone ice sheet models, Cryosphere, 14, 2331–2368, https://doi.org/10.5194/tc-14-2331-2020, 2020.

Nowicki, S. M., Payne, A., Larour, E., Seroussi, H., Goelzer, H., Lipscomb, W., Gregory, J., Abe-Ouchi, A., and Shepherd, A.: Ice Sheet Model Intercomparison Project (ISMIP6) contribution to CMIP6, Geoscientific Model Development, 9, 4521–4545, https://doi.org/10.5194/gmd-9-4521-2016, 2016.

Palmer, M. D., Gregory, J. M., Bagge, M., Calvert, D., Hagedoorn, J. M., Howard, T., Klemann, V., Lowe, J. A., Roberts, C. D., Slangen, A. B., and Spada, G.: Exploring the Drivers of Global and Local Sea-Level Change Over the 21st Century and Beyond, Earth's Future, 8, https://doi.org/10.1029/2019EF001413, 2020.

https://doi.org/10.5194/tc-2021-348
Preprint. Discussion started: 24 November 2021

Pritchard, H. D., Ligtenberg, S. R., Fricker, H. A., Vaughan, D. G., Van Den Broeke, M. R., and Padman, L.: Antarctic ice-sheet loss driven by basal melting of ice shelves, Nature, 484, 502–505, https://doi.org/10.1038/nature10968, 2012.

Rignot, E. and Jacobs, S. S.: Rapid bottom melting widespread near antarctic ice sheet grounding lines, Science, 296, 2020–2023, https://doi.org/10.1126/science.1070942, 2002.

Rignot, E., Mouginot, J., Scheuchl, B., Van Den Broeke, M., Van Wessem, M. J., and Morlighem, M.: Four decades of Antarctic ice sheet mass balance from 1979–2017, Proceedings of the National Academy of Sciences of the United States of America, 116, 1095–1103, https://doi.org/10.1073/pnas.1812883116, 2019.

Sadai, S., Condron, A., DeConto, R., and Pollard, D.: Future climate response to Antarctic Ice Sheet melt caused by anthropogenic warming, Science Advances, 6, 1–9, https://doi.org/10.1126/sciadv.aaz1169, 2020.

Seroussi, H., Nowicki, S., Payne, A. J., Goelzer, H., Lipscomb, W. H., Abe-Ouchi, A., Agosta, C., Albrecht, T., Asay-Davis, X., Barthel, A., Calov, R., Cullather, R., Dumas, C., Galton-Fenzi, B. K., Gladstone, R., Golledge, N. R., Gregory, J. M., Greve, R., Hattermann, T., Hoffman, M. J., Humbert, A., Huybrechts, P., Jourdain, N. C., Kleiner, T., Larour, E., Leguy, G. R., Lowry, D. P., Little, C. M., Morlighem, M., Pattyn, F., Pelle, T., Price, S. F., Quiquet, A., Reese, R., Schlegel, N. J., Shepherd, A., Simon, E., Smith, R. S., Straneo, F., Sun, S., Trusel, L. D., Breedam, J. V., Van De Wal, R. S., Winkelmann, R., Zhao, C., Zhang, T., and Zwinger, T.: ISMIP6 Antarctica: A multi-model ensemble of the Antarctic ice sheet evolution over the 21st century, Cryosphere, 14, 3033–3070, https://doi.org/10.5194/tc-14-3033-2020, 2020.

Shepherd, A., Ivins, E., Rignot, E., Smith, B., van den Broeke, M., Velicogna, I., Whitehouse, P., Briggs, K., Joughin, I., Krinner, G., Nowicki, S., Payne, T., Scambos, T., Schlegel, N., A, G., Agosta, C., Ahlstrøm, A., Babonis, G., Barletta, V., Blazquez, A., Bonin, J., Csatho, B., Cullather, R., Felikson, D., Fettweis, X., Forsberg, R., Gallee, H., Gardner, A., Gilbert, L., Groh, A., Gunter, B., Hanna, E., Harig, C., Helm, V., Horvath, A., Horwath, M., Khan, S., Kjeldsen, K. K., Konrad, H., Langen, P., Lecavalier, B., Loomis, B., Luthcke, S., McMillan, M., Melini, D., Mernild, S., Mohajerani, Y., Moore, P., Mouginot, J., Moyano, G., Muir, A., Nagler, T., Nield, G., Nilsson, J., Noel, B., Otosaka, I., Pattle, M. E., Peltier, W. R., Pie, N., Rietbroek, R., Rott, H., Louise Sandberg-Sørensen, Ingo Sasgen, H. S., Scheuchl, B., Schrama, E., Schröder, L., Seo, K.-W., Simonsen, S., Slater, T., Spada, G., Sutterley, T., Talpe, M., Tarasov, L., van de Berg, W. J., van der Wal, W., van Wessem, M., Vishwakarma, B. D., Wiese, D., and Wouters, B.: Mass balance of the Antarctic Ice Sheet from 1992 to 2017, Nature, 558, 219–222, https://doi.org/10.1038/s41586-018-0179-y, http://www.nature.com/articles/s41586-018-0179-y, 2018.

Thompson, A. F., Stewart, A. L., Spence, P., and Heywood, K. J.: The Antarctic Slope Current in a Changing Climate, Reviews of Geophysics, 56, 741–770, https://doi.org/10.1029/2018RG000624, 2018.

van de Wal, R. S., Zhang, X., Minobe, S., Jevrejeva, S., Riva, R. E., Little, C., Richter, K., and Palmer, M. D.: Uncertainties in Long-Term Twenty-First Century Process-Based Coastal Sea-Level Projections, Surveys in Geophysics, 40, 1655–1671, https://doi.org/10.1007/s10712-019-09575-3, https://doi.org/10.1007/s10712-019-09575-3, 2019.

van den Broeke, M.: Strong surface melting preceded collapse of Antarctic Peninsula ice shelf, Geophysical Research Letters, 32, 1–4, https://doi.org/10.1029/2005GL023247, 2005.